JOURNAL OF THERMOPHYSICS AND HEAT TRANSFER
Vol. 7, No. 2, April–June 1993

Discrete Ordinates Solutions for Radiatively Participating Media in a Cylindrical Enclosure

Slah Jendoubi*
University of Minnesota, Minneapolis, Minnesota 55455
HaeOk Skarda Lee†
NASA Lewis Research Center, Cleveland, Ohio 44135
and
Tae-Kuk Kim‡
Chung-Ang University, Seoul 156-756, Republic of Korea

The radiative transfer equation is solved by the *S-N* discrete ordinates method in the two-dimensional *r-z* coordinates system. The walls of the enclosure are diffuse, and the participating medium absorbs, emits, and anisotropically scatters the radiative energy. Diffuse wall incidence, isothermal medium emission, and collimated incidence problems are considered. Effects of the scattering phase functions on average incident radiation and net radiative heat fluxes are studied. In addition, the effects of scattering albedo, optical thickness, and the wall emissivity are briefly discussed.

Nomenclature

A_e, A_w = east and west control volume surface areas, m^2
a = aspect ratio (H/R)
aa, bb, cc = spatial differencing weights
B_n, B_s = north and south control volume surface areas, m^2
C_j = expansion coefficients of the phase function
E = emissive power, kW/m^2
G = normalized average incident radiation
H = half of the cylinder height, m
I = radiative intensity, kW/(m^2-sr)
M = total number of ordinate directions
MR, MZ = number of grid points in r and z directions
N = order of the *S-N* approximation
$NN + 1$ = number of terms in a phase function expansion
$P_j(\cos\varphi)$ = Legendre polynomial of order j
Q = normalized radiative heat flux
R = cylinder radius, m
r, z = coordinates, m
S = source function, kW/(m^2-sr)
V_p = volume of a control volume, m^3
β = extinction coefficient, m^{-1}
$\delta(\Omega_c - \Omega)$ = Dirac delta function
ε = emissivity
μ, ξ, η = direction cosine in r, z, and ϕ directions
σ = scattering coefficient, m^{-1}
τ = optical thickness (βr or βz)
$\Phi(\Omega'; \Omega)$ = phase function
ϕ, θ = azimuthal and polar angles
φ = scattering angle
Ω = ordinate direction (μ, ξ, η)
ω = scattering albedo (σ/β)

Subscripts
b = blackbody
c = collimated
m = angular azimuthal index
p = center of the control volume

Received Oct. 21, 1991; presented as Paper 92-0123 at the AIAA 30th Aerospace Sciences Meeting, Reno, NV, Jan. 6–9, 1992; revision received May 4, 1992; accepted for publication May 6, 1992.

*Graduate Research Assistant, Department of Mechanical Engineering.
†Aerospace Engineer, Propulsion Systems Division. Member AIAA.
‡Assistant Professor, Department of Mechanical Engineering.

Introduction

THE two-dimensional *r-z* radiative transfer equation is solved by the *S-N* discrete ordinates method for a finite cylinder. The medium enclosed by the cylinder is gray, and it absorbs, emits, and anisotropically scatters the radiative energy. The system geometry for the cylinder of radius R and height $2H$ is illustrated in Fig. 1. The side wall ($r = R$), the bottom wall ($z = 0$), and the top wall ($z = 2H$) are gray, isothermal, and diffusely emit and reflect the radiative energy. The centerline ($r = 0$) is treated as a fictitious, perfectly specular reflecting boundary. A normal collimated radiation beam can be incident at the upper wall of the cylinder, while maintaining the symmetry required for two-dimensional *r-z* solutions. Although the code developed for this study is more flexible, only the results for uniform medium temperature and properties will be presented in this article. The wall boundary conditions are also taken to be uniform over each top, bottom, or side-wall surface. Under these conditions, extending the height to infinity makes the problem one-dimensional radial.

In a previous work, the radiative transfer equation was solved by the integral transformation technique and the F_N

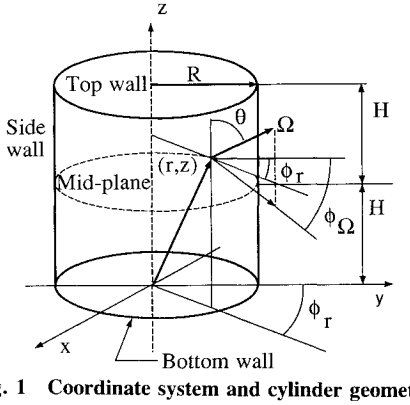

Fig. 1 Coordinate system and cylinder geometry.

method in one-dimensional radial coordinate system for the isotropic scattering case with internal heat generation and diffusely emitting and reflecting surfaces.[1] The integral form of the radiative transfer equation for an isotropic scattering medium in one-dimensional cylindrical coordinates was developed by Thynell and Özisik[2] for an externally incident radiation and diffuse emitting and reflecting boundaries with internal source generation. A year later the solution for this equation was obtained using appropriate expansion functions.[3] Results for uniform externally incident radiation and a parabolic source within the medium were also presented. Low-order *S-N* discrete ordinates methods (*S*-4 and *S*-6) were used to solve the radiative transfer equation in one-dimensional cylindrical geometry with anisotropic scattering and variable properties.[4]

The discretized form of the radiative transfer equation in two-dimensional cylindrical geometry was reported by Fiveland.[5] A low-order *S-N* discrete ordinates method (*S*-4) was used to solve the isotropic scattering equation for two limiting cases: 1) one-dimensional cylindrical, and 2) one-dimensional parallel plates. In 1988, Jamaluddin and Smith[6] developed two-dimensional radiation codes using *S*-2 and *S*-4 discrete ordinates approximations. A low-order *P-N* spherical harmonics approximation results (*P*-3) for two-dimensional cylindrical system were reported by Mengüç and Viskanta[7] for a high temperature, high optical thickness medium with linear anisotropic scattering phase function. Also in the same year, Mengüç and Viskanta[8] published a paper using the delta-Eddington phase function. Numerical solutions were obtained using finite difference and finite element schemes.

The source function, flux, and intensity at the boundaries of a finite two-dimensional cylindrical medium exposed to a Gaussian beam of radiation were reported by Crosbie and Dougherty.[9] The effects of the optical thickness and scattering albedo were studied for the isotropic scattering case. In 1985, a normal collimated beam of Bessel function type was also made incident at the upper surface for linear anisotropic scattering phase function.[10] Recently, general three-dimensional integral formulations of the radiative transfer in scattering media were presented with sample applications in one-dimensional planar and two-dimensional rectangular geometries.[11,12]

The effect of the phase function was reported to be an important factor in anisotropic scattering media.[13,14] The availability of anisotropic scattering solutions of the radiative transfer equation is usually restricted to one-dimensional plane parallel media[15,16] and two-dimensional rectangular problems.[13,14] The solutions for two-dimensional cylindrical problems are few in number and restricted to isotropic or linear anisotropic scattering media.[5,7-10] Therefore, accurate solutions of the radiative transfer equation with more general anisotropic scattering media are needed.

Since cylindrical geometry is closer to many geometries of interest than the two-dimensional rectangular geometry, the code developed for this study can be applied in a variety of situations where particles of different size, volume concentration, and optical properties are present. Among these are nuclear reactors safety, combustion chamber performance, laser beams used for diagnostics, and heat transfer in porous media.

The radiative transfer equation for the cylindrical problems is presented in the next section. A brief discussion of the numerical method used for this analysis is then given. In the discussion of the results, the heated side-wall problem results are presented first. The isothermal emission problem is then briefly discussed. A final set of results compares the collimated and diffuse incidences from the top wall.

Radiative Transfer Equation

For problems involving collimated incidence, the actual intensity (I_a) is expressed as a sum of the diffuse scattered intensity I, and the exponential decay through the medium of the collimated intensity I_c that is incident into the medium through the top wall:

$$I_a(r, z, \Omega) = I(r, z, \Omega) + I_c \exp[-(\tau_{2H} - \tau_z)]\delta(\Omega_c - \Omega) \quad (1)$$

The z location at the top wall is specified as τ_{2H}, and Ω is the direction of the radiative intensity. When only diffuse radiation is incident, the actual intensity is equal to I, the diffuse scattered intensity. The other variables are defined in the Nomenclature.

The system geometry used in this study is shown in Fig. 1. Gray, uniform properties media will be considered for all the cases in this study. The *r-z* two-dimensional equation of radiative transfer for the scattered intensity is given as[5,8,17]

$$\left[\frac{1}{\beta}\left(\mu\frac{\partial}{\partial r} - \frac{\eta}{r}\frac{\partial}{\partial \phi} + \xi\frac{\partial}{\partial z}\right) + 1\right] I(r, z, \Omega) = S(r, z, \Omega) \quad (2)$$

where $\phi = \phi_\Omega - \phi_r$ is the difference in the azimuthal angles shown in Fig. 1. The source function is written as follows:

$$S(r, z, \Omega) = (1 - \omega)I_b[T(r, z)] + \frac{\omega}{4\pi}\int_{4\pi} \Phi(\Omega'; \Omega)I(r, z, \Omega')\, d\Omega' + \frac{\omega}{4\pi} I_c\Phi(\Omega_c; \Omega) \exp[-(\tau_{2H} - \tau_z)] \quad (3)$$

where Ω_c is the direction of collimated incidence, which must be in line with the z axis for this two-dimensional analysis.

The scattering phase function in Eq. (3) is expressed by a Legendre polynomial series as

$$\Phi(\Omega'; \Omega) = \Phi(\cos\varphi) = \sum_{j=0}^{NN} C_j P_j(\cos\varphi) \quad (4)$$

Figure 2 shows the four phase functions to be considered for this study and also used by Kim and Lee[14] who gave the expansion coefficients. *B*1 and *B*2 are the backward-scattering phase functions. *F*2 and *F*3 are the forward-scattering phase functions. *F*3 is the forward-scattering equivalent of the backward-scattering phase function *B*2 (only the sign of C_1 is changed). The isotropic scattering phase function, which is not shown in Fig. 2, is a horizontal line of magnitude of unity. The asymmetry factors are 0.66972, 0.4, −0.18841, and −0.4 for the phase functions *F*2, *F*3, *B*1, and *B*2, respectively.

The appropriate boundary conditions for the diffuse scattered intensity are written for the diffusely emitting and reflecting walls. The bottom wall intensity also includes the

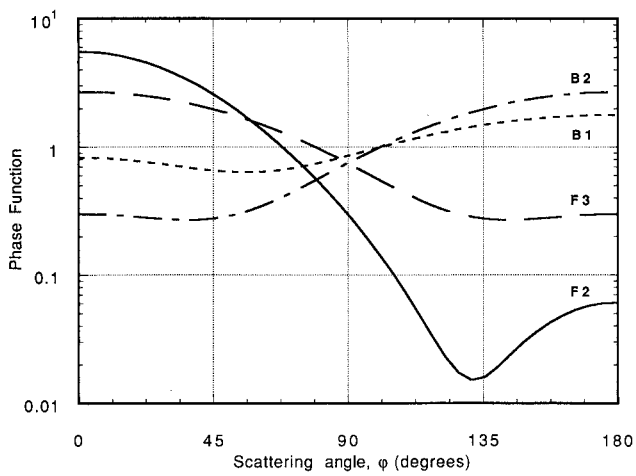

Fig. 2 Phase function vs scattering angle.

reflected component of the collimated incidence that reaches the bottom wall. The symmetry boundary at $r = 0$ is treated as a fictitious wall that is a perfect, specular reflector.

Equations (2) and (3) are solved with the boundary conditions for the diffuse intensity in the cylindrical enclosure. The actual intensity is obtained by applying Eq. (1). Once the actual intensity field is obtained, the normalized radiative fluxes Q_r, Q_z, and normalized average incidence intensity G, are obtained as

$$Q_r(r, z) = \frac{q_r(r, z)}{E_{bb}} = \frac{1}{E_{bb}} \int_{4\pi} \mu I_a(r, z, \Omega)\, d\Omega \quad (5a)$$

$$Q_z(r, z) = \frac{q_z(r, z)}{E_{bb}} = \frac{1}{E_{bb}} \int_{4\pi} \xi I_a(r, z, \Omega)\, d\Omega \quad (5b)$$

$$G(r, z) = \frac{g(r, z)}{I_{bb}} = \frac{1}{4\pi I_{bb}} \int_{4\pi} I_a(r, z, \Omega)\, d\Omega \quad (5c)$$

where the normalization constant E_{bb} is the maximum emissive power for a diffuse incidence problem or the collimated wall heat flux, $|\xi_c| I_c$ ($\xi_c = -1.0$ for this study). I_{bb} is E_{bb}/π for diffuse incidence problems and equal to I_c for the collimated incidence problem.

Numerical Method

The *S-N* discrete ordinates method solves the equation of transfer by replacing the integral in the source function [Eq. (3)] with a quadrature sum and finite differencing the spatial derivatives in Eq. (2). The calculation domain is divided into $MR \times MZ$ control volumes. M is the total number of directions in the hemisphere. Fully symmetric quadrature sets are used in this study. Because no axis receives preferential treatment, the quadrature sets are the same as those used in our previous *x-y* solutions.[13,18]

The discretized equation of transfer for an ordinate direction m is obtained as

$$\mu_m(A_e I_{e,m} - A_w I_{w,m}) + \xi_m(B_n I_{n,m} - B_s I_{s,m}) + (A_e - A_w)\frac{\alpha_{m+1/2} I_{p,m+1/2} - \alpha_{m-1/2} I_{p,m-1/2}}{w_m} + \beta V_p I_{p,m} = \beta V_p S_m \quad (6)$$

where

$$S_m = (1 - \omega) I_b(T_p) + \frac{\omega}{4\pi} \sum_{m'=1}^{M} I_{p,m'} \Phi_{m'm} w_{m'} + \frac{\omega}{4\pi} \Phi_{m_c,m} I_c \exp[-(\tau_{2H} - \tau_p)] \quad (7)$$

is the control volume source function, and the parameters with subscript p are calculated at the center of the control volume. The $w_{m'}$ are the weights associated with each direction Ω'. The angular differencing coefficients $\alpha_{m\pm1/2}$ defined by Carlson and Lathrop[19] as flow terms from the "edges" or "surfaces" of the directional cell are used to approximate the angular intensity distribution. These coefficients are evaluated from

$$\alpha_{m+1/2} = \alpha_{m-1/2} - \mu_m w_m \quad (8)$$

with the first $\alpha_{m-1/2}$ taken as zero at each ξ level. The subscripts e, w, n, s in Eq. (6) refer to the compass directions that indicate quantities at the boundaries of the p control volume. $\Phi_{m',m}$ is the phase function between the direction $\Omega_{m'}$ and Ω_m calculated based on Eq. (4). The direction of the collimated incidence is noted by the subscript m_c, i.e., $\mu_c = 0$, $\eta_c = 0$, $\xi_c = -1$.

Equations (6) and (7) form a system of equations that has more unknowns than the number of equations. Therefore, the solution requires the weighted relationships of the cell (control volume) and boundary averaged intensities. These equations take the following form:

$$aa I_{w,m} + (1 - aa) I_{e,m} = I_{p,m} \quad \text{for } \mu < 0 \quad (9a)$$

$$bb I_{s,m} + (1 - bb) I_{n,m} = I_{p,m} \quad \text{for } \xi < 0 \quad (9b)$$

$$cc I_{p,m+1/2} + (1 - cc) I_{p,m-1/2} = I_{p,m} \quad (9c)$$

Equation (9c) holds for all the directions, while Eqs. (9a) and (9b) need to be rewritten as the direction cosines change sign.

A scheme which guarantees positive values of the radiative intensity is derived by Jendoubi[20] following the guidelines given by Lathrop.[21] The required expressions for $\mu > 0$ and $\xi > 0$ are given as

$$1 - aa' = \frac{\mu_m A_w}{2\xi_m B_n + 2(A_e - A_w)\alpha_{m+1/2}/w_m + \beta V_p} \quad (10a)$$

$$1 - bb' = \frac{\xi_m B_s}{2\mu_m A_e + 2(A_e - A_w)\alpha_{m+1/2}/w_m + \beta V_p} \quad (10b)$$

$$1 - cc' = \frac{(A_e - A_w)\alpha_{m-1/2}/w_m}{2\mu_m A_e + 2\xi_m B_n + \beta V_p} \quad (10c)$$

with $aa = \max(aa', 0.5)$; $bb = \max(bb', 0.5)$; and $cc = \max(cc', 0.5)$. Appropriate sign changes in directions must be incorporated for different sweep directions.

The discretized equations also involve $I_{m\pm1/2}$. The initial $I_{m-1/2}$ for each ξ level is set equal to the first $I_{p,m}$ for each control volume. Simple algebraic equations can then be written for each sweep direction and used to build a numerical code that solves for $I_{p,m}$. Iterative solutions are required since the source term S_m is itself a function of the volume average intensity $I_{p,m}$. A convergence criterion of less than 0.0001% change in the intensities is used. Additional information on the quadrature set, the sweeping scheme, and other details of the numerical technique can be found in Jendoubi.[20]

Results and Discussions

Three kinds of problems are considered in this section; 1) diffuse incidence, 2) isothermal emission, and 3) normal collimated incidence. The results are presented in terms of normalized average incident radiation [(Eq. (5c)] and normalized net radiative heat fluxes [Eqs. (5a) and (5b)] at the boundaries and at the midplane of the cylinder.

The aspect ratio, defined as $a = H/R$, is equal to 1.0 for all the figures except for Figs. 3 and 4. The optical radius, τ_R

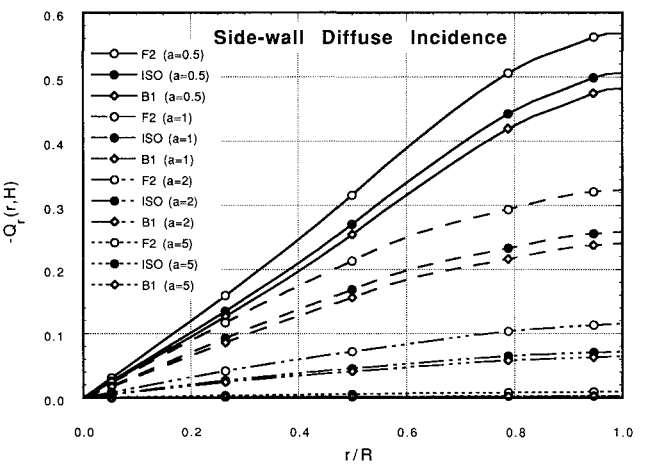

Fig. 3 Effect of the aspect ratio and scattering phase function on the midspan $-Q_r(r, H)$.

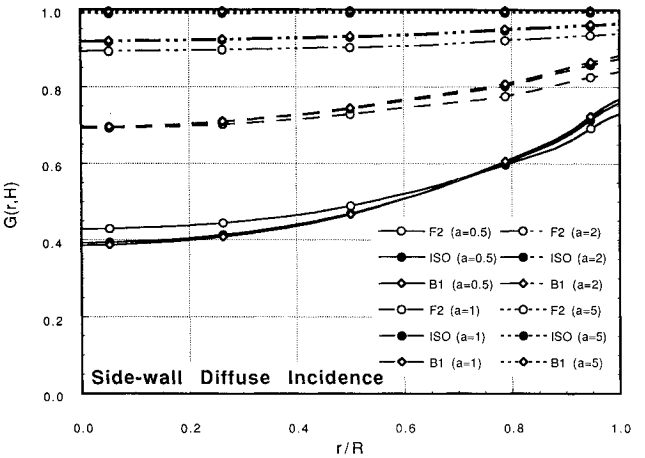

Fig. 4 Effect of the aspect ratio and scattering phase function on the midplane $G(r, H)$.

$= \beta \times R$, is equal to 1.0 in all the figures except for Fig. 7 where the τ shown in the legend are τ_R.Wall emissivities are all 1.0 for the solutions shown in these figures except for Fig. 12. Other emissivity values were tested and discussed in Jendoubi.[20] The different scattering albedo values considered are indicated in the discussion for each figure. All the presented results are computed using the S-14 approximation.

Side-Wall Diffuse Incidence

For all the figures presented in this section, the side wall (wall 2) is hot (E_2 = positive constant), and all other walls and the medium are cold. All walls are black. The effect of the aspect ratio and the scattering phase function are illustrated in Figs. 3 and 4. The midspan $-Q_r(r, H)$ is shown in Fig. 3, and $G(r, H)$ is shown in Fig. 4 for a pure scattering medium with $\omega = 1$. There is no absorption or emission for such a medium.

The heat flux distributions in Fig. 3 show that the forward-scattering phase function $F2$ transfers the most amount of net energy from the hot side wall ($r/R = 1$) into the cold medium for all aspect ratios considered. The backward scattering phase function $B1$ transfers the least amount of energy, with the isotropic scattering phase function results serving as idealized reference values.

All the cases shown in Fig. 3 assume a unity normalized flux incidence at the hot wall that is directed toward the centerline. The net radiative heat flux is then determined by subtracting the amount of radiation directed back toward the hot wall from the opposite parts of the hot wall and from scattering in the medium. The net heat flux values are the highest for the lowest aspect ratio case with the shortest hot side wall length, because there is then the smallest flux directed back toward the hot wall at the midplane. As the aspect ratio increases, more energy is transferred back toward the hot wall, and the symmetry of this pure scattering problem forces the net heat flux toward zero in the one-dimensional limit of infinite aspect ratio. The solutions for an aspect ratio of 5 already show nearly the one-dimensional limit.

Figure 4 shows the midplane average incident radiations for the identical cases as shown in Fig. 3. As the aspect ratio is increased by increasing the height of the cylinder while keeping the radius constant, the average incident radiation increases toward the exact one-dimensional result of unity for this pure scattering medium. This increase is due to the additional energy coming from the extra length of the hot wall with the increase in the aspect ratio. Figure 4 shows a significant change of the average incident radiation as the aspect ratio changes from 0.5 to 1.0 to 2. The average incident radiation changes slowly with a further increase in the aspect ratio beyond 2. Beyond an aspect ratio of about 5, no more energy will be sensed at the midplane of the cylinder, even if the height is increased. The problem therefore becomes one-dimensional.

Figure 4 also shows that for any phase function the average level of radiative intensity decreases toward the centerline due to the lack of intensity contributions from the cold end-walls. Since uniform, unity normalized-intensity irradiation form the hot wall into the medium is assumed, the level of $G(r, H)$ near the hot wall is determined by the amount of intensity directed back toward the hot wall. For all aspect ratios considered, $G(r, H)$ are higher near the hot side-wall with the backward scattering phase function $B1$ because it tends to scatter back more energy toward the heated wall. This trend of the $B1$ phase function showing the highest average level of intensity continues throughout the midplane for all aspect ratios greater than 0.5. For the aspect ratio of 0.5, the backscattering effect is diminished toward the centerline of the medium due to the small optical thickness in the z direction. Away from the hot wall region, the back-scattering effect is smaller than the effect of forward scattering phase function $F2$ in increasing the transmitted intensities from the hot sidewall toward the centerline.

For $\omega = 1$, Fig. 5 shows the net radial heat flux plotted along the side wall for all five phase functions considered for this study. The figure shows that far away from the end walls the forward-scattering phase functions give larger heat fluxes than the backward-scattering phase functions. The differences in the results are small at the ends of the cylinder.

In Fig. 6, the end-wall normalized net axial radiative heat flux Q_z is plotted vs r/R for $\omega = 1$. The net heat flux is leaving the medium and gained by the end walls. Q_z is therefore positive at the top wall and negative at the bottom wall, but they are equal in magnitude due to the symmetry of the prob-

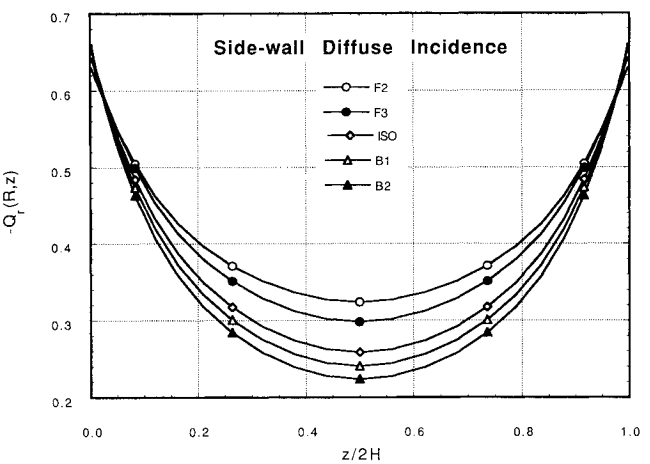

Fig. 5 Scattering phase function comparisons of the side wall $-Q_r(R, z)$.

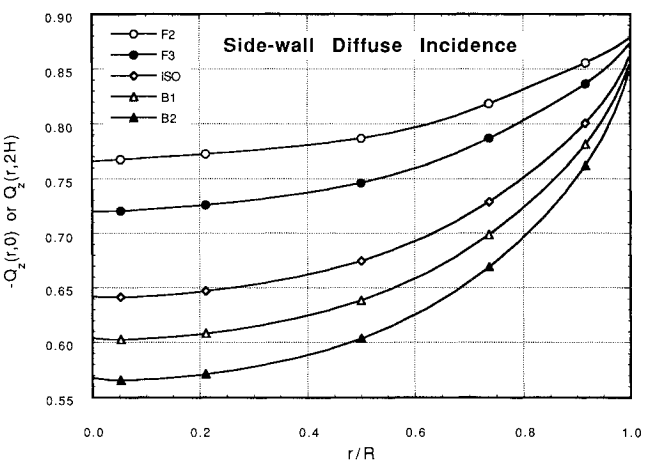

Fig. 6 Scattering phase function comparisons of the end wall Q_z.

lem. Because the forward-scattering phase functions tend to scatter more energy in the forward direction away from the source of energy at the side wall, the higher heat fluxes delivered to the end walls are given by $F2$ and $F3$. The lower heat fluxes are given by the backward-scattering phase functions $B1$ and $B2$.

The effect of the optical thickness is shown in Fig. 7 for the forward-scattering phase function $F3$ and an absorbing medium with $\omega = 0.5$. The net heat flux leaving the hot side wall and being absorbed by the medium is plotted vs $z/2H$. As the optical thickness increases for $a = 1$, more medium will be enclosed by the cylinder. Therefore, more energy will be supplied by the hot wall and absorbed by the cold medium for larger optical thicknesses.

Isothermal Medium Emission

The walls of the cylinder are cold and black for this case. The isothermal gray medium is hot, and it absorbs, emits, and anisotropically scatters the radiative energy.

The lack of importance of the phase function anisotropy for this problem is illustrated by using the phase functions $F2$, $F3$, isotropic, $B1$, and $B2$. In Fig. 8 the average incident radiation is plotted as a function of $z/2H$ along the side wall. This figure with an expanded scale shows that at the midplane ($z/2H = 0.5$) the differences in the average incident radiation given by the different phase functions are very small. Near the end walls, the forward-scattering phase functions give slightly higher average incident radiation because they scatter more energy toward the end walls. The phase function effects are unimportant, because the medium emission is isotropic. If the scattering albedo is high enough to show phase function effects ($\omega = 0.8$ for Fig. 8), the emission is very small.

Figure 9 illustrates the important effect of the scattering albedo on the side wall, normalized average incident radiation $G(R, z)$ for the phase function $F2$. The figure shows the decrease in the average incident radiation as the scattering albedo increases, as well as the symmetry about the location $z/2H = 0.5$. As the scattering albedo increases, less energy will be emitted by the medium and be available for transmission to the side wall. Although not shown, the net radial radiative heat flux also decreases as the scattering albedo increases because of the decrease in the medium emission.

Top Wall Collimated vs Diffuse Incidence

The comparison between the collimated incidence and diffuse incidence results are considered in this section. Either a normal collimated incidence through a transparent top wall or a top-wall diffuse incidence is considered. All other walls and the gray medium are cold. All walls are nonreflecting with respect to the radiation inside the enclosure. Only the bottom wall is allowed to reflect radiation to show the emissivity effect in Fig. 12.

The z component of the normalized net heat flux at the bottom wall is plotted vs r/R in Fig. 10 for both diffuse and collimated incidence ($\omega = 1.0$). $-Q_z(r, 0)$ is shown in the figure because the energy from the top wall is going through the medium and gained by the bottom wall. The curves start at high values at the center of the cylinder and decay as r increases due to the loss of energy to the cold side wall. The figure shows that the forward-scattering phase functions transmit more energy to the bottom wall. The radiation given by the diffuse incidence is smaller than that given by the collimated incidence. This is because for the diffuse incidence, most of the radiation leaving the top wall is at different angles

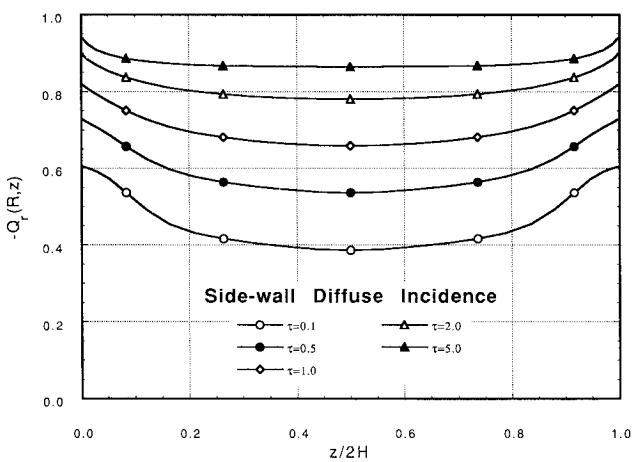

Fig. 7 Effect of optical thickness on the side wall $-Q_r(R, z)$.

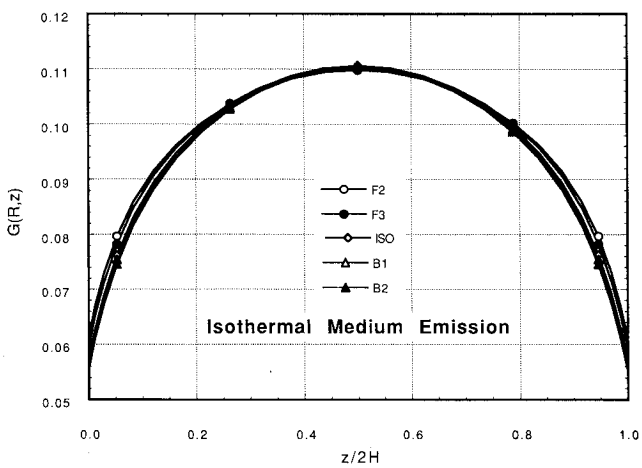

Fig. 8 Scattering phase function comparisons of the side wall $G(R, z)$.

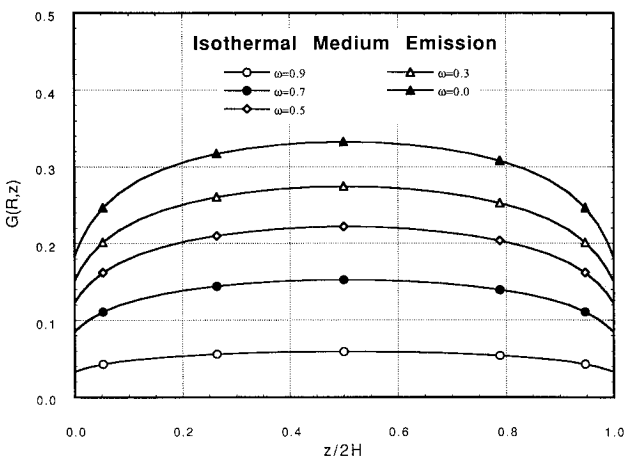

Fig. 9 Effect of scattering albedo on the side wall $G(R, z)$.

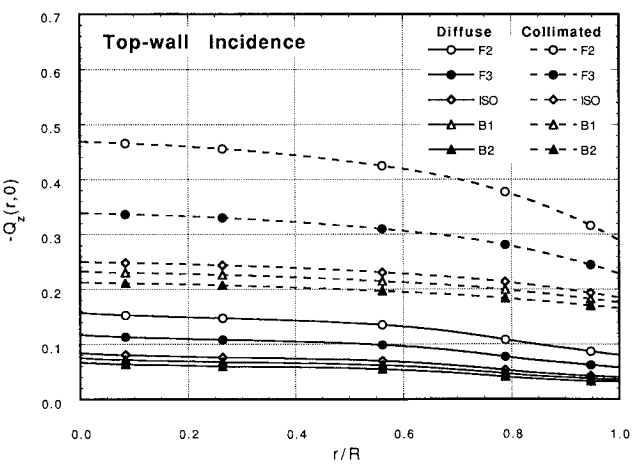

Fig. 10 Scattering phase function comparisons of the bottom wall $-Q_z(r, 0)$.

from the downward, or $-z$ direction and will be absorbed by the side wall before reaching the bottom wall.

The side-wall normalized net heat flux is plotted as function of $z/2H$ in Fig. 11 for $\omega = 1.0$. For the diffuse incidence case, the highest net heat flux gained by the side wall is given by the backward-scattering phase function $B2$ near the top wall. In contrast, the forward-scattering function $F2$ gives the largest net heat flux to the side wall far away from the top wall. The results for the collimated incidence case are quite different from those of the diffuse incidence case. The figure shows that for all the phase functions, the heat fluxes at the bottom ($z/2H = 0.0$) increase toward the top wall where the collimated incidence occurs. After reaching maximum values, the fluxes start to decrease near the top wall. The position where the maximum heat flux occurs is closer to the bottom wall as the asymmetry factor increases, or the phase function becomes more peaked in the forward direction. This is because the radiation leaving the top wall has to travel a certain distance depending on the phase function before it can be scattered to the side wall. For the highly forward-scattering phase functions the minimum radial heat flux occurs at $z/2H = 1.0$. For the backward-scattering phase functions the minimum values occur at $z/2H = 0$. The maximum heat flux is given by the isotropic scattering phase function, because it scatters the energy equally in all directions.

The effect of the wall emissivity on the normalized net radiative heat flux Q_r is shown in Fig. 12 for $\omega = 0.7$ and isotropic scattering medium. For this figure, the side wall is black and cold ($E_2 = 0.$). Only the bottom wall (wall 4) is gray and cold, and it diffusely reflects the radiative energy ($E_4 = 0$, $\varepsilon_4 = \varepsilon$). The net radial heat flux Q_r at the side wall is plotted as a function of $z/2H$. The energy transmitted through the medium and absorbed by the side wall increases slightly as the emissivity decreases because of the increase in the reflected energy from the bottom wall. This increase in heat flux is more pronounced near the bottom wall than near the top wall. For the collimated incidence case, the high emissivity curve of Q_r vs $z/2H$ has only one peak near the top of the cylinder. The low emissivity curves have two peaks, one at the bottom wall and the other near the top wall.

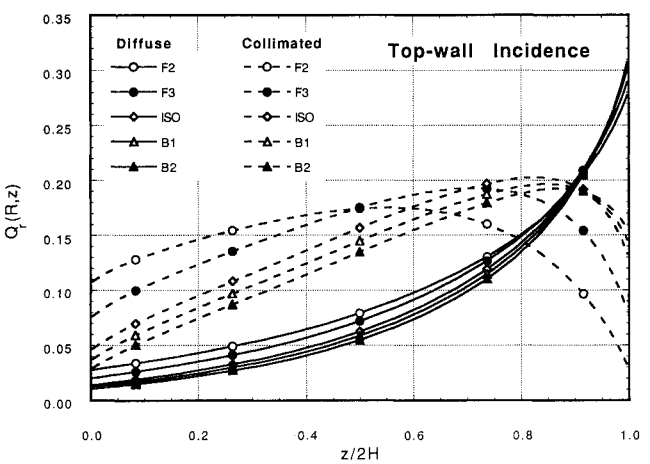

Fig. 11 Scattering phase function comparisons of the side wall $Q_r(R, z)$.

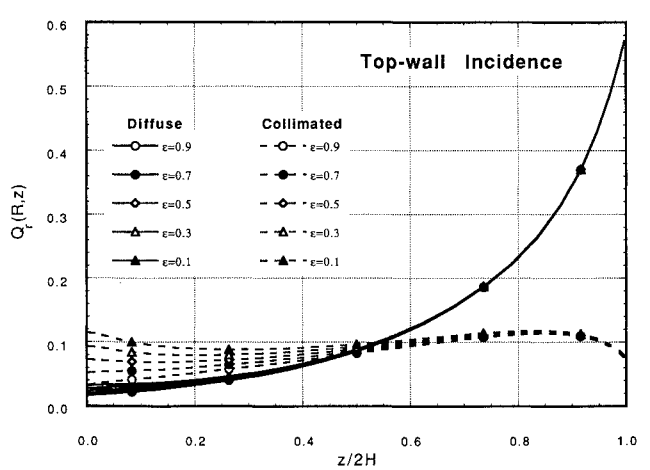

Fig. 12 Effect of emissivity on the side wall $Q_r(R, z)$.

Conclusions

The S-N discrete ordinates method is used to solve the radiative transfer equation in two-dimensional cylindrical coordinates. The walls are gray and diffusely emit and reflect the radiative energy. The participating medium is gray, and it absorbs, emits, and anisotropically scatters the radiative energy. The anisotropic phase functions are expanded into finite series of Legendre polynomials.

For symmetric problems, the intensity levels are more sensitive to the order of the S-N discrete ordinates method than the flux solutions. For problems with highly anisotropic scattering medium, a higher order S-N approximation is needed which does require more computation effort. For a typical case ($\omega = 1.0$, $\tau_R = 1$, $a = 1$, $F2$ phase function, side-wall diffuse incidence), approximately 40 s of Cray X-MP cpu time is required for a S-14 solution vs the approximately 6 s required for an S-6 solution.

The phase function anisotropy is found to have a significant effect on the average incident radiation and heat flux, for both diffuse and collimated incidences. For isothermal emission problems, however, the phase function has a very small effect on both radiative quantities. In general, the backward-scattering phase functions scatter back more energy toward the source of energy than the forward-scattering phase functions which tend to scatter energy away from the energy source. The scattering albedo and optical thickness have significant effects on the radiative transfer for all the cases studied. The bottom reflecting wall has almost no effect for the top wall diffuse incidence problem and is only significant near the bottom wall for the case of collimated top-wall incidence.

Acknowledgments

This work was supported in part by the National Science Foundation Grant NSF/CBT-8451076. A grant from the Minnesota Supercomputer Institute is also gratefully acknowledged.

References

[1]Siewert, C. E., and Thomas, G. R., Jr., "Radiative Transfer Calculations in Spheres and Cylinders," *Journal of Quantitative Spectroscopy and Radiative Transfer*, Vol. 34, No. 1, 1985, pp. 59–64.

[2]Thynell, S. T., and Özisik, M. N., "Integral Form of the Equation of Transfer for an Isotropically Scattering, Inhomogeneous Solid Cylinder," *Journal of Quantitative Spectroscopy and Radiative Transfer*, Vol. 36, No. 6, 1986, pp. 497–503.

[3]Thynell, S. T., and Özisik, M. N., "Radiative Transfer in Absorbing, Emitting, Isotropically Scattering, Homogeneous Cylindrical Media," *Journal of Quantitative Spectroscopy and Radiative Transfer*, Vol. 38, No. 6, 1987, pp. 413–426.

[4]Tsai, J. R., and Özisik, M. N., "Radiation in Cylindrical Symmetry with Anisotropic Scattering and Variable Properties," *International Journal of Heat and Mass Transfer*, Vol. 33, No. 12, 1990, pp. 2651–2658.

[5]Fiveland, W. A., "A Discrete Ordinates Method for Predicting Radiative Heat Transfer in Axisymmetric Enclosures," American Society of Mechanical Engineers, 82-HT-20, 1982.

[6]Jamaluddin, A. S., and Smith, P. J., "Predicting Radiative Transfer in Axisymmetric Cylindrical Enclosures Using the Discrete Ordinates Method," *Combustion Science and Technology*, Vol. 62, Nos. 4–6, 1988, pp. 173–186.

[7]Megüç, M. P., and Viskanta, R., "Radiative Transfer in Axisymmetric, Finite Cylindrical Enclosures," *Journal of Heat Transfer*, Vol. 108, No. 2, 1986, pp. 271–276.

[8]Mengüç, M. P., and Viskanta, R., "Radiation Transfer in a Cylindrical Vessel Containing High-Temperature Corium Aerosols," *Nuclear Science and Engineering*, Vol. 92, No. 4, 1986, pp. 570–583.

[9]Crosbie, A. L., and Dougherty, R. L., "Two-Dimensional Isotropic Scattering in a Finite Thick Cylindrical Medium Exposed to a Laser Beam," *Journal of Quantitative Spectroscopy and Radiative Transfer*, Vol. 27, No. 2, 1982, pp. 149–183.

[10]Crosbie, A. L., and Dougherty, R. L., "Two-Dimensional Linearly Anisotropic Scattering in a Finite Thick Cylindrical Medium Exposed to a Laser Beam," *Journal of Quantitative Spectroscopy and Radiative Transfer*, Vol. 33, No. 5, 1985, pp. 487–520.

[11]Tan, Z., "Radiative Heat Transfer in Multidimensional Emitting, Absorbing, and Anisotropic Scattering Media—Mathematical Formulation and Numerical Method," *Journal of Heat Transfer*, Vol. 111, No. 1, 1989, pp. 141–147.

[12]Wu, C.-Y., "Exact Integral Formulation for Radiative Transfer in an Inhomogeneous Scattering Medium," *Journal of Thermophysics and Heat Transfer*, Vol. 4, No. 4, 1990, pp. 425–431.

[13]Kim, T.-K., and Lee, H., "Effect of Anisotropic Scattering on Radiative Heat Transfer in Two-Dimensional Rectangular Enclosure," *International Journal of Heat and Mass Transfer*, Vol. 31, No. 8, 1988, pp. 1711–1721.

[14]Kim, T.-K., and Lee, H., "Radiative Heat Transfer in Two-Dimensional Anisotropic Scattering Media with Collimated Incidence," *Journal of Quantitative Spectroscopy and Radiative Transfer*, Vol. 42, No. 3, 1989, pp. 225–238.

[15]Flicke, C., "The Phase-Integral Method for Radiative Transfer Problems with Highly Peaked Phase Function," *Journal of Quantitative Spectroscopy and Radiative Transfer*, Vol. 20, 1978, pp. 429–445.

[16]Garcia, R. D. M., and Siewert, C. E., "Benchmark Results in Radiative Transfer," *Transport Theory and Statistical Physics*, Vol. 14, No. 4, 1985, pp. 437–483.

[17]Özisik, M. N., *Radiative Transfer and Interactions with Conduction and Convection*, Wiley-Interscience, New York, 1973.

[18]Lathrop, K. D., and Brinkley, F. W., "TWOTRAN-II: An Interfaced Exportable Version of the TWOTRAN Code for Two-Dimensional Transport," Los Alamos Scientific Lab. Rept., LA-4848-MS, July 1973.

[19]Carlson, B. G., and Lathrop, K. D., "Transport Theory—The Method of Discrete Ordinates," *Computing Methods in Reactor Physics*, edited by H. Greenspan, C. N. Kelber, and D. Okrent, Gordon & Breach, New York, 1968, pp. 165–266.

[20]Jendoubi, S., "Radiative Transfer Solutions for Cylindrical Coordinates with Emitting, Absorbing and Anisotropic Scattering Medium," M.S. Thesis, Univ. of Minnesota, Minneapolis, MN, Sept. 1991.

[21]Lathrop, K. D., "Spatial Differencing of the Transport Equation: Positivity vs Accuracy," *Journal of Computational Physics*, Vol. 4, 1969, pp. 475–498.